Jacobsen catalyst anchored onto an activated carbon as an enantioselective heterogeneous catalyst for the epoxidation of alkenes

3 AUTHORS, INCLUDING:

Cristina Freire
University of Porto
230 PUBLICATIONS **3,187** CITATIONS

RESEARCH ARTICLE

Hybrid photochromic multilayer films based on chitosan and europium phosphomolybdate

Diana M. Fernandes · Cristina Freire

Abstract Multilayer films based on chitosan and $K_{11}[Eu^{III}(PMo_{11}O_{39})_2]$ were prepared on different substrates using the layer-by-layer method. UV–Vis spectra of the films showed regular stepwise growth. X-ray photoelectron spectroscopy data confirmed the presence of chitosan and phosphomolybdate within the films and scanning electron microscopy images revealed a completely covered surface with a roughened texture. The film electrochemical responses and permeability were studied by cyclic voltammetry. Films revealed four surface-confined Mo-based reduction processes ($Mo^{VI} \rightarrow Mo^V$). Studies with $[Fe(CN)_6]^{3-/4-}$ and $[Ru(NH_3)_6]^{3+/2+}$ showed that film permeability depended on the film thickness and on the charge of the outer layer. Irradiation of films with UV light confirmed their photochromic properties through the colour change from transparent to blue. Colouration–discolouration cycles could be repeated up to 36 cycles without the loss of optical contrast, indicating high film photochromic stability. These results provided valuable insights for exploring the potential application of polyoxometalate-based films for the construction of photochromic devices.

Keywords Layer-by-layer films · Phosphomolybdates · Electrochemistry · Photochromism · Chitosan

D. M. Fernandes · C. Freire (✉)
REQUIMTE/Departamento de Química e Bioquímica,
Faculdade de Ciências, Universidade do Porto, 4169-007 Porto,
Portugal
e-mail: acfreire@fc.up.pt

1 Introduction

Photochromic compounds have been the focus of intensive investigations for several decades because of their potential applications in optical memory devices, optical switches and chemical sensors [1–3]. The majority of the photochromic materials are organic (ca. diarylethene [4] and spiropyrans [5] derivatives), but inorganic compounds can also exhibit these outstanding properties. Transition-metal oxides (ca. tungsten oxide, molybdenum oxide, titanium dioxide, vanadium pentoxide) [6] and polyoxometalates (POMs) [2, 3, 7, 8] are known to exhibit photochromism; however, in some cases they showed poorer photochromic responses compared to organic photochromic compounds. It has been shown that the combination of POMs with proton donor organic counter ions resulted in improved colour reversibility and response time [3, 9]. This class of hybrid organic–inorganic photochromic materials is promising for practical applications due to their rich structures, chemical and physical properties, cost-effective synthesis, high colouration contrast and tunable optical properties. The photochromism mechanism was rationalized in terms of intermolecular hydrogen donation combined with intramolecular electron transfer [2].

For the application of inorganic clusters in photochromic devices they need to be processed into films. The layer-by-layer (LbL) assembly technique has been proven to be a promising methodology for fabricating uniform and ultrathin film [10, 11]. Functional components, including transition-metal complexes, surfactants, nanoparticles and polymers, can be assembled orderly into multilayer films by the LbL method, since this methodology allows for a high degree of control over composition, thickness and supermolecular architectures.

Chitosan is the deacetylated form of chitin, which is a structural polysaccharide encountered in the shells of crabs and in the exoskeleton of shrimps and other arthropods. It has attracted considerable interest due to its potential application in material [12–14], biological and industrial sciences [15–17]. It has a pK_a of 6.2, being insoluble in alkaline and neutral solutions, but it is able to dissolve into an acidic media becoming highly positively charged due to the protonation of the amine groups. Due to this fact it has been widely used in the fabrication of multilayer films by LbL technique, combined with anionic polymers and polyanions like the POMs, where adsorption is predominantly governed by electrostatic attraction between the oppositely charged layers. Some of the films prepared with chitosan and POMs showed electrochromic [18] and electrocatalytic applications [12, 19] and antibacterial activity [20].

In this article, we report the successful fabrication of hybrid multilayer films based on chitosan and potassium salt of lanthanide-bridged phosphomolybdate, $K_{11}[Eu^{III}(PMo_{11}O_{39})_2]$, using the electrostatic LbL self-assembly method. The film growth was monitored by UV–Vis spectroscopy, the composition was evaluated by X-ray photoelectron spectroscopy (XPS) and surface morphology was examined by scanning electron microscopy (SEM). The electrochemical behaviour of the multilayer films and film permeability towards the redox probes $[Fe(CN)_6]^{3-/4-}$ and $[Ru(NH_3)_6]^{3+/2+}$ was studied by cyclic voltammetry and their photochromic properties under UV irradiation evaluated.

2 Experimental

2.1 Reagents and solutions

Sodium acetate (99.5 % Merck), acetic acid (100 % Merck) and potassium chloride were used as received. Medium molecular weight chitosan was purchased from Sigma-Aldrich with a deacetylation degree of 75–85 %. Potassium salt of $Eu(PMo_{11})_2$ was prepared following an adapted method from the literature [21, 22]; a detailed characterization of this compound is described in Ref. [23]. Potassium hexacyanoferrate(III) and hexamminorutheni-um(III) solutions (1.0 mM) were prepared by dissolving the appropriate amount of $K_3[Fe(CN)_6]$ and $[Ru(NH_3)_6]Cl_3$ in 1 M KCl.

Electrolyte solutions for voltammetry were prepared using ultra-pure water (resistivity 18.2 MΩ cm at 25 °C, Millipore). Acetate buffer solutions with different pH values, used for electrochemical studies of the LbL films, were prepared by mixing appropriate amounts of CH_{3}COOH 0.1 mol dm^{-3} and CH_3COONa 0.1 mol dm^{-3}.

The chitosan solution used to build-up the chitosan/POM films was prepared dissolving 1 g chitosan in 0.5 dm^{-3} ultra-pure water and 1 g of acetic acid with stirring for 2 h.

2.2 Instrumentation

Electronic spectra of the multilayer films were recorded on a Varian cary 50 Bio spectrophotometer in the range 190–1,000 nm, at room temperature, using quartz slides.

SEM analysis was performed at the Centro de Materiais da Universidade do Porto (CEMUP), Portugal, in high-vacuum conditions, using a high-resolution (Schottky) environmental scanning electron microscope (ESEM) with X-ray microanalysis and backscattered electron diffraction pattern analysis (FEI Quanta 400FEG/EDAX Genesis X4M). Before SEM measurements, a thin Au layer was deposited on the top of the samples to prevent charging problems.

The XPS measurements were performed at CEMUP (Porto, Portugal), in a VG Scientific ESCALAB 200A spectrometer using non-monochromatized Al K_α radiation (1486.6 eV). To correct possible deviations caused by electric charge of the samples, the C 1s band at 285.0 eV was taken as internal standard. The XPS spectra were deconvoluted with the XPSPEAK 4.1 software, using nonlinear least squares fitting routine after a Shirley-type background subtraction. The surface atomic percentages were calculated from the corresponding peak areas and using the sensitivity factors provided by the manufacturer.

Cyclic voltammetry measurements were carried out using an Autolab PGSTAT 30 potentiostat/galvanostat (EcoChimie B.V.) controlled by GPES software. Voltammetric measurements were performed at room temperature. A conventional three-electrode compartment cell was used. Two types of working electrodes were used: (i) glassy carbon electrode GCE (3 mm diameter, BAS, MF-2012), combined with platinum wire (7.5 cm, BAS, MW-1032) as auxiliary electrode and Ag/AgCl (sat. KCl) (BAS, MF-2052) as reference electrode, and (ii) indium tin oxide (ITO) coated polyethylene terephthalate (PET) sheet (60 Ω resistance, Aldrich) combined with platinum wire as the auxiliary electrode and Ag/AgCl (sat. NaCl) (Methrohm, ref: 6.0724.140) as reference electrode. The cell was enclosed in a grounded Faraday cage and kept under flowing argon during experiments. A combined glass electrode (Crison) connected to a pH meter Basic 20$^+$ (Crison) was used for the pH measurements.

Photochromic experiments of were conducted using a CN-6 darkroom equipped with a 6 W UV lamp (λ = 254 nm) as the light source (Vilber Lourmat).

2.3 Film preparation

The chitosan/POM multilayer films were deposited on the following substrates: quartz slides for UV–Vis

measurements, glass slides for XPS and glassy carbon and ITO/PET electrodes for cyclic voltammetry studies. Quartz slides were cleaned by placing them in a H_2SO_4/H_2O_2 (3:1) (v/v) hot bath ($\sim 80\ ^{\circ}C$) for 30 min and then in a $H_2O/H_2O_2/NH_3\cdot H_2O$ (5:1:1) (v/v/v) hot bath ($\sim 80\ ^{\circ}C$) for 40 min. The cleaned quartz slides were then rinsed with ultra-pure water and dried under a stream of pure argon. After the cleaning step, the quartz slides were immersed initially in a 1 g dm^{-3} (pH 2.5) chitosan solution for 10 or 20 min followed by rinsing with water and dried under argon. The chitosan-coated substrates were then immersed into a 5.0×10^{-4} mol dm^{-3} Eu(PMo$_{11}$)$_2$ solution in pH 2.5 acetate buffer for 10 or 20 min, also followed by rinsing and dried under argon. This procedure was repeated as many times as the number of bilayers pretended.

For the glass slides the same solution treatments were used, but for just 1–2 min. The ITO/PET electrodes were cleaned by washing then with acetone. The GCE was conditioned by a polishing/cleaning procedure prior to coating: it was polished with aluminium oxide of particle size 0.3 μm (Buehler-Masterprep) on a microcloth polishing pad (BAS Bioanalytical Systems Inc.), and then the electrode was rinsed with ultra-pure water and finally sonicated for 5 min. The multilayer films were build-up on the surface of glass slides, ITO/PET and GCE electrodes using the same methodology as described above for the quartz slides but using deposition times of 10 min for each sipping solution.

2.4 Photochromic studies

The choice of the irradiation time to be used in the photochromic cycles was determined by exposing the {chitosan/Eu(PMo$_{11}$)$_2$}$_{15}$ multilayer films to UV lamp ($\lambda = 254$ nm) using different irradiation times: 0, 5, 10, 30 and 45 min; immediately after irradiation, the film electronic spectra were recorded. The final photochromic cycles were performed using the {chitosan/Eu(PMo$_{11}$)$_2$}$_{15}$ film exposed to UV lamp for 30 min and its electronic spectrum recorded; subsequently, the film was left to rest in the dark overnight and its electronic spectrum recorded after the dark cycle.

3 Results and discussion

3.1 {Chitosan/Eu(PMo$_{11}$)$_2$}$_n$ films building

Figure 1 depicts UV–Vis electronic spectra of {chitosan/Eu(PMo$_{11}$)$_2$}$_n$ film (with $n = 2$–18), sampled after deposition of even number of layers during its assemblage on a quartz substrate using 1 g dm^{-3} of chitosan in pH 2.5 acetate buffer and 5.0×10^{-4} mol dm^{-3} of Eu(PMo$_{11}$)$_2$ in

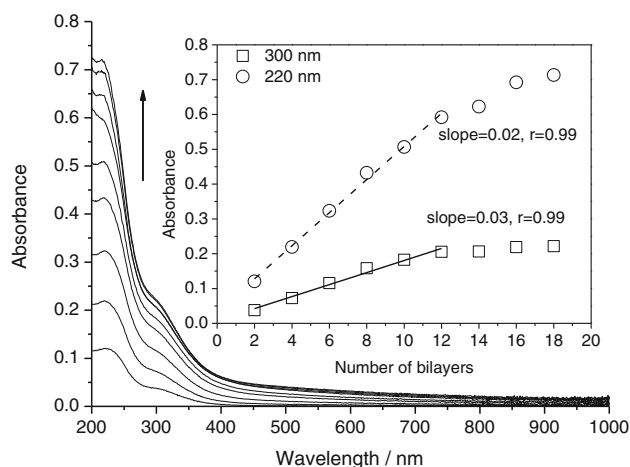**Fig. 1** UV–Vis absorption spectra of {chitosan/Eu(PMo$_{11}$)$_2$}$_n$ multilayers for $n = 2$–18 adsorbed on a quartz slide: 1 g dm^{-3} of chitosan in pH 2.5 acetate buffer and 5.0×10^{-4} mol dm^{-3} of Eu(PMo$_{11}$)$_2$ in pH 2.5 acetate buffer. *Inset* absorbance at $\lambda = 220$ (*circle*) and 300 nm (*square*) as a function of n

pH 2.5 acetate buffer. As the number of bilayers increased there is an increment in the absorbance at $\lambda = 220$ and 300 nm, which is represented in the inset of Fig. 1, as straight lines in the plot of Abs$_{max}$ vs. number of bilayers. The observed electronic bands at $\lambda = 220$ and 300 nm are assigned to oxygen-to-molybdenum charge transfer transitions of Eu(PMo$_{11}$)$_2$ which is being incorporated into film multilayers; chitosan has no electronic bands in this spectral region [24]. The linearity of Abs$_{max}$ vs. number of bilayers plots up to 12 bilayers suggests that the amount of material deposited in each bilayer is constant and consistent with a stepwise and structurally regular growth process for the LbL hybrid film, which is indicative of strong interaction between the charged interlayers [25]. From $n = 12$ to 18, the absorbance values begin to show a negative deviation from linearity (max of 18.6 %). suggesting a lower efficiency on film deposition.

Since the deposition time used in film self-assembly is an important parameter for effective film growth, two values were tested: 10 and 20 min. Figure S1, supplementary data, depicts the plots of Abs$_{max}$ vs. number of bilayers for {chitosan/Eu(PMo$_{11}$)$_2$}$_n$ film (with $n = 2$–14) at $\lambda = 220$ and 300 nm, using the two deposition times for the chitosan and POM solutions. As the absorbance values show no significant differences (≤ 8 %), the lower deposition time (10 min) was selected for the subsequent experiments.

The surface coverage per layer, Γ_{UV}, was estimated from the electronic spectra of the multilayers, using the expression, $\Gamma_{UV} = A_\lambda/2m\varepsilon_\lambda$, where A_λ is the absorbance at the specified wavelength, m is the number of layers and ε_λ is the isotropic molar absorption coefficient (M^{-1} cm^{-1}) [10]; the factor 2 accounts for the fact that the film is covering both sides of the quartz slide. A set of seven solutions
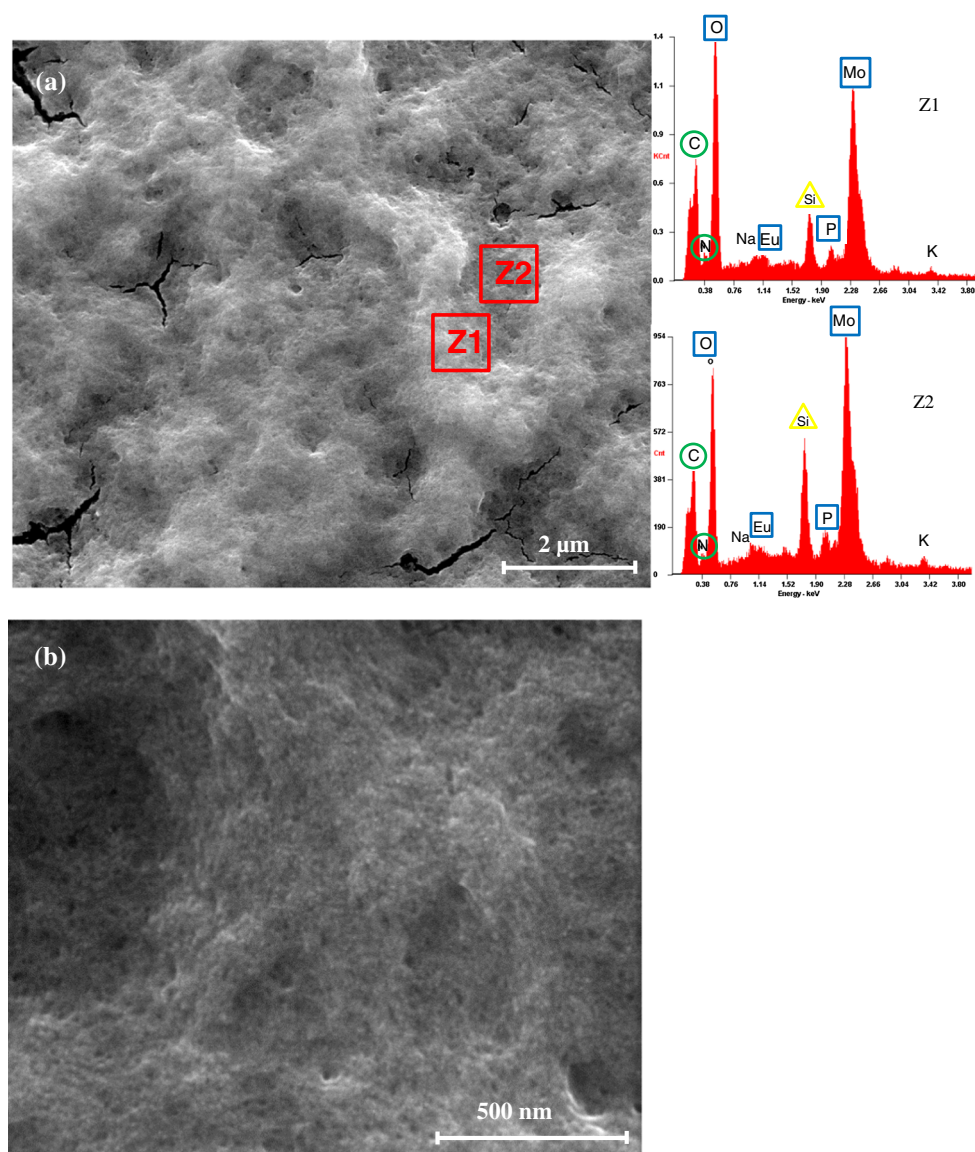
Fig. 2 SEM images of {chitosan/Eu(PMo$_{11}$)$_2$}$_{20}$ multilayers deposited on a glass slide at magnification 25,000× with EDS spectra at two selected zones (**a**) and at magnification 150,000× (**b**)

of each compound (1.0×10^{-6}–4.0×10^{-5} mol dm^{-3}) in acetate buffer was used to determine the isotropic molar absorption coefficient and the value obtained was 9.89×10^4 M^{-1} cm^{-1}, leading to $\Gamma_{UV} = 0.253 \pm 0.031$ nmol cm^{-2} for a {chitosan/Eu(PMo$_{11}$)$_2$}$_n$ film assembled on a quartz substrate using 1 g dm^{-3} of chitosan in pH 2.5 acetate buffer (10 min) and 5.0×10^{-4} mol dm^{-3} of Eu(PMo$_{11}$)$_2$ in pH 2.5 acetate buffer (10 min).

3.2 SEM and XPS analysis

Figure 2 shows SEM images of {chitosan/Eu(PMo$_{11}$)$_2$}$_{20}$ films deposited on a glass slide at two different magnifications. It is possible to see that the surface is completely covered with a roughened texture that can be tentatively ascribed to the Eu(PMo$_{11}$)$_2$ entrapment by the chitosan chains. It is also likely that POM aggregates to a certain level as the cationic polymer chitosan may have reduced the coulombic repulsion of adjacent POM centres; a similar behaviour was reported for a multilayer film of [P$_2$W$_{18}$O$_{62}$]$^{6-}$ and a Ru-metallodendrimer [26]. The cracks observed in Fig. 2a can be attributed partly to the effect of the vacuum in the SEM chamber and also, to a greater extent, to the high-energy beam (on increasing the magnification, cracks were formed in places where they did not exist previously). Figure 2a also shows the EDS analysis for different film areas which confirms the presence of the

Table 1 Core-level binding energies of each component for multilayer film of {chitosan/Eu(PMo$_{11}$)$_2$}$_{15}$ obtained by curve fitting of XPS spectra and respective surface atomic percentages

Compound	Binding energy (BE)[a]					
	C 1s	O 1s	N 1s	P 2s	Eu 3d$_{5/2}$ (Eu^{3+}/Eu^{2+})	Mo 3d$_{3/2}$ + 3d$_{5/2}$ (Mo^{6+}/Mo^{5+})
{Chitosan/ Eu(PMo$_{11}$)$_2$}$_{15}$ film	285.0 (1.8)	531.0 (2.1)	400 (1.4)	190.3 (2.9)	1134.8 (4.9)	236.8 (2.2) + 233.7 (2.2)
	286.8 (1.8)	532.9 (2.1)	402 (1.4)		1124.4 (4.9)	235.4 (2.2) + 232.3 (2.2)
	288.6 (1.8)	534.5 (2.1)				
	Atomic %[b]					
	63.0	30.0	0.9	0.5	0.2	5.4

[a] The values between brackets refer to the FWHM of the bands

[b] Determined by the areas of the respective bands in the high-resolution XPS spectra

two film components in both areas (darker and lighter): peaks due to C and N are from the chitosan polymer while P, O, Mo and Eu correspond to the POM; the Si peak corresponds to the substrate.

Film thickness was evaluated through SEM images (Fig. S2, supplementary data). It is possible to see that there are areas with different heights and consequently different film thickness: measurements were made in 15 points and gave an average value of 1.487 μm.

In Table 1 are the summarized XPS data obtained for {chitosan/Eu(PMo$_{11}$)$_2$}$_{15}$ films; the deconvoluted XPS spectra of multilayer films are shown in Fig. S3, supplementary data, as an example.

The presence of elements of each film component: chitosan (C, N) and POM (P, Mo, O and Eu) confirms the successful fabrication of the hybrid films. On the other hand, the absence of Na and K (counter ions) indicates that the film charge mechanism has only the contribution from the intrinsic charge compensation arising from the film layers.

The presence of N and its atomic percentage could be assessed but with low certainty due to the overlap of N 1s and Mo 3p peaks in the N 1s spectrum. Nevertheless, the spectrum was fitted taking into consideration the existence of Mo 3p (3p$_{1/2}$ and 3p$_{3/2}$) and N 1s peaks. The area obtained through modulation of Mo 3p is similar to that obtained for Mo 3d, suggesting a correct fitting of peaks taking into consideration the N 1s peaks. The two peaks in the N 1s spectrum are due to the presence of two types of nitrogen atoms in the multilayer films: one is attributed to the amine groups of chitosan (–NR$_2$) at 400 eV and the other at 402 eV corresponds to protonated amine groups.

The C 1s spectrum (Fig. S3a) was fitted with three peaks at 285.0, 286.8 and 288.6 eV. The peak at 285 eV is attributed to the aliphatic carbon (–C–C– or –C–H–), that at 286.8 eV to carbon bonded to the amine groups (–C–NR$_2$, where R is C or H) [27]; the peak at 288.6 eV can be ascribed to residual organic impurities (CO$_2$ and carbonate species). The O 1s spectrum was fitted with three peaks at

531.0, 532.0 and 534.5 eV. The former at 531.0 eV can be ascribed to O–Mo, that at 532.9 eV to O–P and the less intense at 534.5 eV to O–Eu [28]. The XPS spectrum of the Mo 3d is shown in Fig. S3d. The binding energies of Mo 3d can be resolved into 3d$_{5/2}$ and 3d$_{3/2}$ doublets caused by spin-orbital coupling. Upon deconvolution of the spectra, the curves are fitted with two couples of binding energies for Mo^{5+} (232.3 and 235.4 eV) and Mo^{6+} (233.7 and 236.8 eV). The presence of Mo^{5+} species suggests that photoreduction of POMs occurred when the sample was exposed to the X-ray source, as already observed in previous work [29]. However, in this case the percentage of Mo^{5+} species (72 %) relative to Mo^{6+} present is higher than those obtained for films prepared by the LbL methodology with this POM or SiW$_{11}$ analogues [30]. The main difference is the type of polymer used, consequently these results suggest that the presence of chitosan in the films facilitates the photoreduction of POMs when the film is exposed to the X-ray source.

Europium analysis was performed using 3d XPS high-resolution spectrum because of the overlapping of P 2p peak with the Eu 4d. The XPS spectrum of Eu 3d shows two doublets: that at 1134.8 and 1164.6 eV is attributed to 3d$_{5/2}$ and 3d$_{3/2}$ of Eu^{3+}, while the other that appears at 1124.4 and 1154.2 eV is ascribed to Eu^{2+} 3d$_{5/2}$ and 3d$_{3/2}$, which is in agreement with previously published values [14, 31, 32]. For surface atomic % only the 3d$_{5/2}$ region was considered. The atomic % ratios Eu:P of $\sim$1:2, P:Mo of 1:11 and 1:22 for Eu:Mo confirm that the POM structure is maintained in the LbL films.

3.3 Electrochemical characterization of the multilayer films

The cyclic voltammograms for a single {chitosan/Eu(PMo$_{11}$)$_2$} bilayer obtained at different scan rates in pH 4.0 CH$_3$COOH/CH$_3$COONa are shown in Fig. 3. Since chitosan is not electroactive in the potential range studied, the electrochemical responses are attributed to the immobilized POMs and
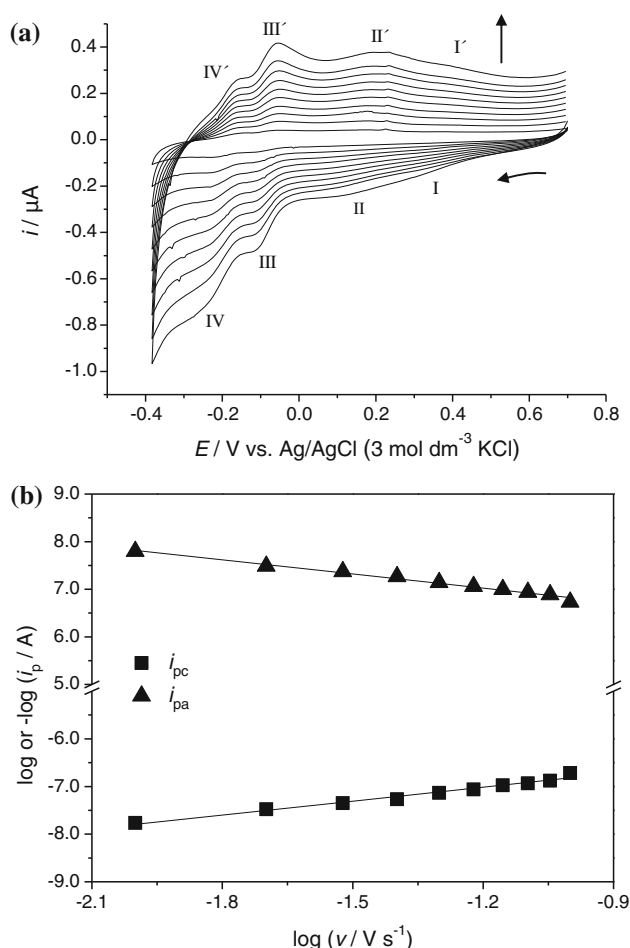
(a)

(b)

Fig. 3 Cyclic voltammograms of {chitosan/Eu(PMo$_{11}$)$_2$} bilayer in pH 4.0 CH$_3$COOH/CH$_3$COONa at different scan rates: 0.01, 0.02, 0.03, 0.04, 0.05, 0.06, 0.07, 0.08, 0.09, and 0.1 V s^{-1}. Adsorbed on a GCE: 1 g L^{-1} chitosan in pH 2.5 CH$_3$COOH solution, 10 min; 0.5×10^{-3} mol dm^{-3} of Eu(PMo$_{11}$)$_2$ in pH 2.5 CH$_3$COOH/CH$_3$CO-ONa, 10 min (**a**); plots of log i_{pc3} (*filled square*) and i_{pa3} (*filled triangle*) vs. log v (**b**)

correspond to Mo-centred reduction processes (Mo^{VI} → Mo^{V}): $E_{pc1} = 0.332$, $E_{pc2} = 0.131$, $E_{pc3} = -0.108$ and $E_{pc4} = -0.233$ V vs. Ag/AgCl. At pH 4.0 H$_2$SO$_4$/Na$_2$SO$_4$ buffer solution, the free POM also revealed four pairs of peaks at $E_{pc1} = 0.480$, $E_{pc2} = 0.290$, $E_{pc3} = -0.125$ and $E_{pc4} = -0.295$ V vs. Ag/AgCl [33]. The electrochemical response of {chitosan/Eu(PMo$_{11}$)$_2$} shows the first two reduction processes at more negative potentials compared with the same processes for the free POM in solution. However, further reductions processes (peaks 3 and 4) occur at more positive potentials in the immobilized POM rather than in solution, suggesting, in this case a kinetic facilitation of the reduction processes when the POM is immobilised: protonated chitosan facilitates the Mo redox processes since the positive charges of chitosan help to prevent the build-up of negative charge. It must be referred that the first reduction processes at more positive values (peaks 1
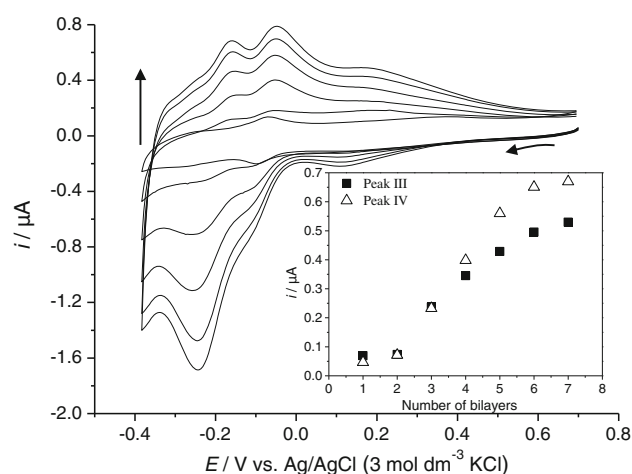
and 2) are not influenced by pH of the solution, in opposition to the reduction processes at more negative potentials (peaks 3 and 4) that are pH-dependent [33].

In the experimental timescale employed (scan rates in the range 0.01–0.1 V s^{-1}) the values of peak potential did not change with scan rate. Figure 3b depicts the plot of log i_p vs. log v for {chitosan/Eu(PMo$_{11}$)$_2$} bilayer film. The cathodic and anodic peak currents of Mo waves were directly proportional to the scan rate (with $r = 0.992$), which indicates a surface-confined process [34]. In addition, the anodic/cathodic peak-to-peak separation (ΔE_p) for the molybdenum waves was ca. 0.048–0.057 V.

The representative cyclic voltammograms as a function of the number of layers for {chitosan/Eu(PMo$_{11}$)$_2$}$_n$ film up to 6 are depicted in Fig. 4. The cathodic and anodic peak potentials did not change with an increase in the number of layers. The inset shows the plots of i_{pc3} and i_{pc4} vs. the number of bilayers (n). From bilayer 1 to 2 no significant differences are observed in the peak currents. From $n = 2$ to 6, the plot shows linear growth, indicating a uniform growth of the film for each deposition. Above these numbers of bilayers, peak currents progressive decrease and the peaks become broad and progressively plateau-shaped. This may suggest a change in the diffusion regime, for example from a strictly surface confined to a solution-type behaviour, with corresponding changes in the movement of charges and counter ions leading to an increased charge-transfer resistance in the supramolecular film structure.

Surface coverage of electroactive species immobilized at electrode surfaces can be calculated from cyclic voltammetry according to the equation $\Gamma = (4i_pRT)/(n^2F^2vA)$ where i_p is the peak current (A), n is the number of electrons transferred, v is the scan rate (V s^{-1}), A is the

Fig. 4 Cyclic voltammograms of {chitosan/Eu(PMo$_{11}$)$_2$}$_n$ multilayers for $n = 0$–7 in pH 4.0 CH$_3$COOH/CH$_3$COONa at 0.05 V s^{-1}. *Inset* shows i_{pc} vs. number of layers for peaks III (*filled square*) and IV (*triangle*)

geometric area of the electrode (0.0725 cm^2 for GCE), R is the gas constant, T is the temperature (298 K) and F is Faraday's constant [34]. The POM surface coverage within the film was estimated using the peak current of E_{pc2} (two electron process) for a single {chitosan/Eu(PMo$_{11}$)$_2$} bilayer; E_{pc2} was plotted against scan rate (0.01–0.1 V s^{-1}) and the value of i_p/v obtained was used to calculate the POM surface coverage, $\Gamma_{POM} = 5.70 \pm 0.37 \times 10^{-3}$ nmol cm^{-2}.

Films were also build-up on ITO/PET electrodes that were then used for stability tests through application of continuous double potentials steps. The cyclic voltammograms obtained (Fig. S4) present some differences when compared with those obtained using a GCE. The cyclic voltammograms show two well-defined two-electron reduction processes with $E_{pc2} = -0.160$ and $E_{pc3} = -0.296$ V and another less defined with E_{pc1} approximately at 0.157 V vs. Ag/AgCl, contrasting with the four peaks observed when a GCE electrode is used. It seems that the first two pairs of peaks merge into a single one and all peaks are shifted towards more negative potentials. Surface-confined processes are still maintained and films also grow uniformly with increasing number of bilayers from $n = 1$ to 6. For much thicker films, there is a significant increase in film resistance, leading to practically electroinactive films; for this reason, no electrochromic studies could be done, since for the thin films that exhibit electroactivity, the POM concentration is not enough to give a significant absorbance.

The stability of the LbL {chitosan/Eu(PMo$_{11}$)$_2$}$_2$ hybrid films was tested through application of continuous double potentials steps (0.7 and −0.4 V, 30 s each). For the first 5,000 s there is a current loss of 57 % (data not shown) which is assigned to the removal of weakly attached, physically adsorbed molecules. Figure S5 displays the current of {chitosan/Eu(PMo$_{11}$)$_2$}$_2$ hybrid films during subsequent double potentials steps from 15,000 to 65,000 s. Results show a current decrease of 9.2 % indicating that the thin films present good electrochemical stability.

Cyclic voltammetry was used to study film permeability properties of the multilayer films towards the negatively charged [Fe(CN)$_6$]$^{3-/4-}$ redox probe and the positively charged [Ru(NH$_3$)$_6$]$^{3+/2+}$. Electrostatic attraction between the multilayer surface and the redox probe (in the case of opposite charges) should facilitate the interfacial electron transfer process, whereas when they have the same charge (electrostatic repulsion) would make the electron transfer reaction more difficult. Many groups have used the [Fe(CN)$_6$]$^{3-/4-}$ redox couple to study the permeability of multilayer films [10, 35–37]. However, studies of electron transfer at films containing POMs are few [10, 38, 39]. It was shown that the permeability towards these species can be tailored through the multilayer construction and
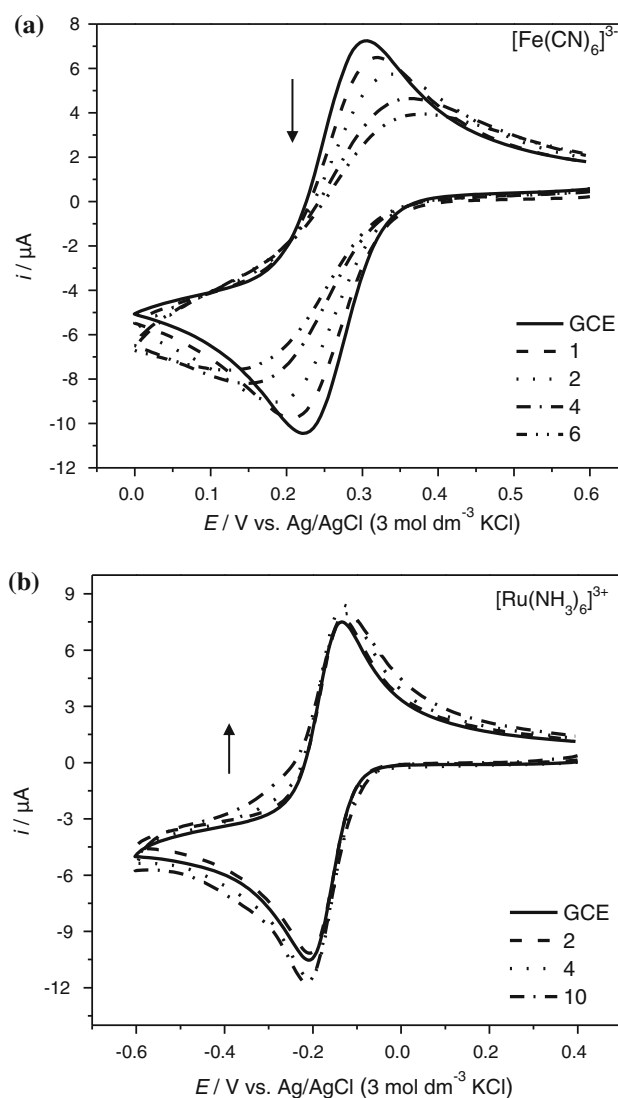

Fig. 5 Cyclic voltammograms of **a** [Fe(CN)$_6$]$^{3-/4-}$ (1 mM, 1 M KCl), $v = 0.050$ V s^{-1}, at modified electrode with {chitosan/Eu(PMo$_{11}$)$_2$}$_n$ for $n = 0, 1, 2, 4,$ and 6; **b** [Ru(NH$_3$)$_6$]$^{3+/2+}$ (1 mM, 1 M KCl) for $n = 0, 2, 4,$ and 10

deposition conditions [10] and the number of multilayer films can influence the shape of the cyclic voltammograms [38].

Figure 5a shows cyclic voltammograms of [Fe(CN)$_6$]$^{3-/4-}$ at the electrode modified with {chitosan/Eu(PMo$_{11}$)$_2$}$_n$ for $n = 0, 1, 2, 4$ and 6. At the bare GCE electrode, [Fe(CN)$_6$]$^{3-/4-}$ shows one cathodic peak and the corresponding anodic peak at $E_{pc} = 0.304$ and $E_{pa} = 0.0228$ V, respectively, assigned to the Fe$^{III/II}$ reduction/oxidation of the probe at the bare electrode. Increasing the number of film bilayers, from 1 to 6, produces drastic and progressive decrease in probe peak current by 10.6–51.4 %. This shows that the increase of bilayers number with a terminal negatively charged Eu(PMo$_{11}$)$_2$ anion leads to a decrease in the number of probe ions that reach the electrode substrate, due to electrostatic

Table 2 Cyclic voltammetric data of $[Fe(CN)_6]^{3-/4-}$ and $[Ru(NH_3)_6]^{3+/2+}$ complexes at bare GCE and modified with $\{chitosan/Eu(PMo_{11})_2\}_n$ films, $v = 0.05$ V s^{-1}; potentials units are in V vs. Ag/AgCl (3 mol dm^{-3} KCl)

Electroactive probe	n	i_{pa} (μA)	i_{pc} (μA)	E_{pa}	E_{pc}	$|\Delta E_p|$	$E_{1/2}^a$	Δi_{pa} (%)[b]
$[Fe(CN)_6]^{3-/4-}$	0	8.44	−8.55	0.297	0.226	0.071	0.262	–
	1	7.54	−7.52	0.311	0.212	0.099	0.262	10.6
	2	6.70	−6.75	0.326	0.198	0.128	0.262	20.6
	3	6.39	−6.32	0.332	0.193	0.139	0.263	24.2
	4	4.97	−5.26	0.350	0.174	0.176	0.262	41.1
	6	4.10	−4.31	0.365	0.165	0.200	0.265	51.4
$[Ru(NH_3)_6]^{3+/2+}$	0	8.62	−8.63	−0.139	−0.206	0.067	−0.173	–
	2	8.60	−8.90	−0.135	−0.206	0.071	−0.171	0.2
	4	9.39	−8.93	−0.135	−0.206	0.071	−0.171	−8.9
	8	9.20	−10.7	−0.125	−0.206	0.085	−0.168	−6.8
	10	8.84	−10.3	−0.125	−0.210	0.125	−0.168	−2.5

[a] $E_{1/2} = E^{\circ\prime} = 0.5(E_{pa} + E_{pc})$
[b] $\Delta i_{pa} = [(i_{pa}(GCE) - i_{pa}(bilayer))/i_{pa}(GCE)] \times 100$

repulsion of $[Fe(CN)_6]^{3-/4-}$ by the negatively charged $Eu(PMo_{11})_2$ anion and the presence of fewer pathways, as film becomes thicker. Similar results were obtained for $[Co_4(H_2O)_2(PW_9O_{34})_2]^{10-}$ clusters [40]. This loss of probe permeability is also similar to that observed at a number of films where polyelectrolytes are used [41].

Besides the effect on the peak current, the $\{chitosan/Eu(PMo_{11})_2\}_n$ film also has a marked influence on redox probe voltammetric i–E curve shape and peak potential separation. The peaks become broad and progressively plateau-shaped with increasing number of bilayers, suggesting a change in the diffusion regime from semi-infinite linear diffusion to convergent diffusion to an array of sites behaving as microelectrodes [41]. There is also an increase in peak potential separation (from 0.071 to 0.200 V, see Table 2), which is attributed to an increase in the film coverage that in turn increases the charge-transfer resistance of the probe redox process. Apart these kinetic and diffusional aspects, the formal potential for the $[Fe(CN)_6]^{3-/4-}$ couple does not change significantly, indicating that there is no measurable influence on the underlying thermodynamics.

When the positively charged $[Ru(NH_3)_6]^{3+/2+}$ redox probe is used at the $\{chitosan/Eu(PMo_{11})_2\}_n$ modified electrode, the changes are not so significant. Figure 5b shows cyclic voltammograms of $[Ru(NH_3)_6]^{3+/2+}$ at the electrode modified with $\{chitosan/Eu(PMo_{11})_2\}_n$ for $n = 0$, 2, 4, 8 and 10. At the bare electrode, the redox probe shows one cathodic peak and the corresponding anodic peak at $E_{pc} = -0.206$ and $E_{pa} = -0.135$ V, respectively, assigned to the $Ru^{III/II}$ reduction/oxidation. For an electrode coated with a single bilayer, the cyclic voltammogram exhibits quasi-reversible properties, indicating that the probe undergoes electron transfer at the underlying electrode surface. Increasing the number of bilayers until $n = 10$ leads to a slight increase in peak currents (<9.0 %) which is due to the electrostatic attraction of $[Ru(NH_3)_6]^{3+/2+}$ by the negatively charged $Eu(PMo_{11})_2$ anion within the film. There is also an increase in peak potential separation for

$n \geq 8$; nevertheless, as for the negative electroactive probe, the formal potential for the $[Ru(NH_3)_6]^{3+/2+}$ couple does not change.

These changes in peak current and peak-to-peak separation when using $[Fe(CN)_6]^{3-/4-}$ or $[Ru(NH_3)_6]^{3+/2+}$ couples indicate that electrostatic attractions or repulsions have significant effects on the kinetics of the redox reactions, either accelerating or decelerating the processes. In order to test the reproducibility of these trials, these were repeated three times and very similar results were obtained: peak position did not change and the relative standard deviation of the peak currents was <4 %.

3.4 Photochromism of $\{chitosan/Eu(PMo_{11})_2\}_n$ films

The electronic spectra of the $\{chitosan/Eu(PMo_{11})_2\}_{15}$ films before and after UV irradiation are displayed in Fig. 6a. Before UV irradiation, no absorption bands of the $\{chitosan/Eu(PMo_{11})_2\}_{15}$ films appear in visible region, because neither chitosan or $Eu(PMo_{11})_2$ shows electronic bands in visible region. After UV light irradiation, a broad absorption band is observed in the range of 450–950 nm and the colour of the films changes from transparent to blue (Fig. 6b, left to right) with increasing irradiation time. This new electronic band, responsible for the blue colour, is assigned to intervalence charge transfer band ($Mo^V \rightarrow Mo^{VI}$) of the POM and is in good agreement with the results in the literature for the electroreduced $Eu(PMo_{11})_2$ in solution [23].

It can also be observed that an increase in the exposition time from 0 to 30 min leads to an increase in the intensity of the new band (~ 200 %) and consequently in the blue colour. The photochromic contrast can be defined as the transmittance change ($\Delta\%T$) at a specified wavelength, where the photochromic material has the highest optical contrast. In the experimental conditions of Fig. 6a, we can see that $\{chitosan/Eu(PMo_{11})_2\}_{15}$ film exhibits 20 % of optical contrast at 745 nm: this result indicates that
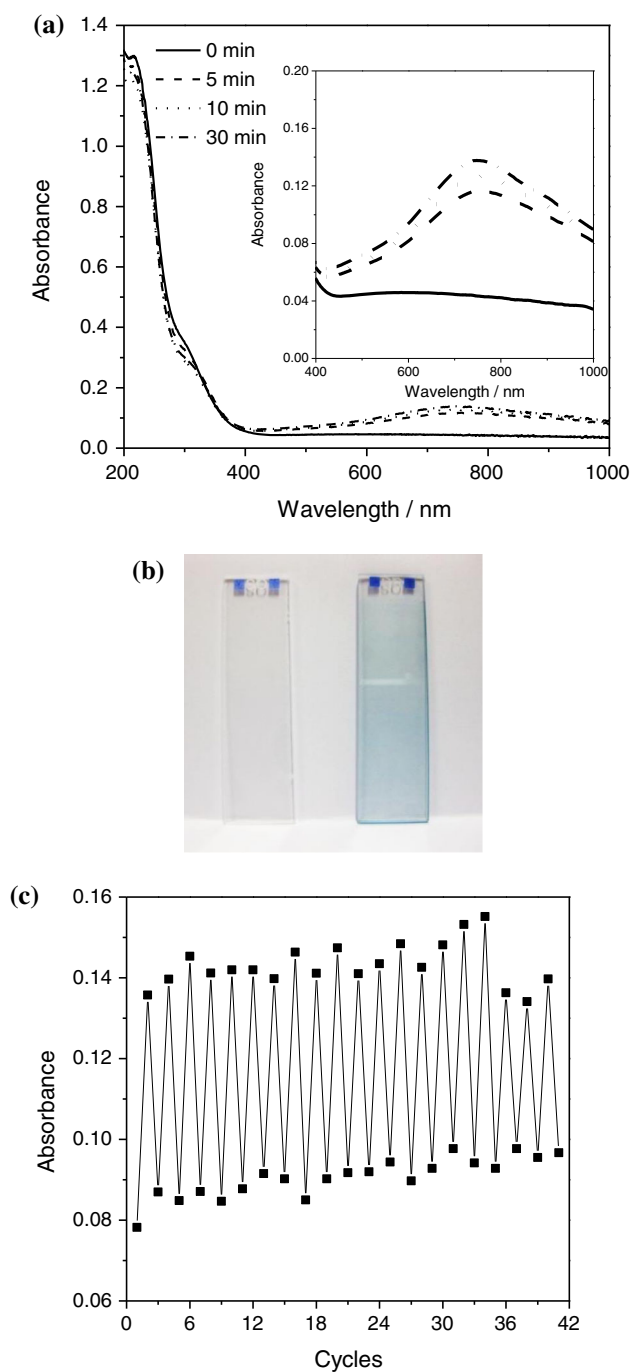
Fig. 6 UV–Vis spectra recorded after different irradiation times (**a**), {chitosan/Eu(PMo$_{11}$)$_2$}$_{15}$ film oxidized (*left*) and reduced (*right*) (**b**), colouration/bleach cycles of the photochromic process for 30 min irradiation time (**c**)

{chitosan/Eu(PMo$_{11}$)$_2$}$_n$ films should be thicker ($n \sim 50$ bilayers) in order to have higher optical contrasts in the range of 70–80 %, values generally accepted for practical applications. When the UV light is taken off, the blue films began to discolour, gradually becoming transparent under ambient conditions, indicating colouring/bleaching reversibility at room temperature [9, 42, 43].

Photoexcitation of the O=Mo ligand to metal charge transfer (LMCT) bands in MoO$_6$ leads to the transfer of a hydrogen from protonated nitrogen of chitosan to the bridge oxygen atom at the photoreduced site in the edge-shared MoO$_6$ octahedral lattice. This is followed by the interaction of one electron with the proton which was transferred to the oxygen atom. At the same time, the hole left at the oxygen atom as a result of the O → Mo LMCT transfer interacts with the nonbonding electrons on the amino nitrogen atom to form a charge transfer complex [2]. The bleaching, which occurs in the presence of O$_2$ molecules, is caused by the back reaction, which is trigged by an electron transfer from Mo^{5+} atom to oxygen molecules [44].

Figure 6c represents the colouration/bleach cycles of the photochromic process. The reversibility of the colouration–discolouration is clearly observed for 18 times (corresponding to 18 days) without almost any loss of colour contrast. The fact that colour change of the hybrid film is reversible for a considerable number of colouration–discolouration cycles (up to 36 cycles), implies a very high photochromic stability of {chitosan/Eu(PMo$_{11}$)$_2$}$_n$ films and suggests potential applications in the areas of photo switches and memory devices.

4 Conclusions

Multilayer films incorporating chitosan and europium phosphomolybdate Eu(PMo$_{11}$)$_2$ were successfully prepared on different substrates using electrostatic LbL self-assembly. Electronic spectroscopy revealed a uniform film growth typical of systems with strong electrostatic interactions between the component layers and XPS established the incorporation of chitosan and POM in the multilayer films and confirms intrinsic film charge compensation.

The multilayer films showed Mo reduction processes due to the POM immobilization and film permeability, accessed using [Fe(CN)$_6$]$^{3-/4-}$ and [Ru(NH$_3$)$_6$]$^{3+/2+}$ as electrochemical probes, revealed that electrostatic attraction and repulsion towards the probes play a significant role on the kinetics of the redox reactions. Photochromic studies showed that upon UV irradiation the {chitosan/Eu(PMo$_{11}$)$_2$}$_n$ multilayer films undergo colour change from transparent to blue as a consequence of the intervalence charge transfer transition between the photoreduced Mo^V to Mo^{VI} ions. Furthermore, the high number of colouration–discolouration cycles reached by {chitosan/Eu(PMo$_{11}$)$_2$}$_n$ films indicates robust and high stable photochromic films. The obtained results provide valuable information for exploring future application of LbL POM-based films for the fabrication of photochromic devices.

References

1. Tsivgoulis GM, Lehn JM (1995) Photonic molecular devices—reversibly photoswitchable fluorophores for nondesctructive readout for optical memory. Angew Chem Int Ed Engl 34(10):1119–1122

2. Yamase T (1998) Photo- and electrochromism of polyoxometalates and related materials. Chem Rev 98(1):307–325. doi:10.1021/cr9604043

3. He T, Yao JN (2006) Photochromism in composite and hybrid materials based on transition-metal oxides and polyoxometalates. Prog Mater Sci 51(6):810–879. doi:10.1016/j.pmatsci.2005.12.001

4. Tian H, Yang SJ (2004) Recent progresses on diarylethene based photochromic switches. Chem Soc Rev 33(2):85–97. doi:10.1039/b302356g

5. Raymo FM, Tomasulo M (2005) Electron and energy transfer modulation with photochromic switches. Chem Soc Rev 34(4):327–336. doi:10.1039/b400387j

6. He T, Yao JN (2004) Photochromism in transition-metal oxides. Res Chem Intermed 30(4–5):459–488. doi:10.1163/1568567041280890

7. Pardo R, Zayat M, Levy D (2011) Photochromic organic–inorganic hybrid materials. Chem Soc Rev 40(2):672–687. doi:10.1039/c0cs00065e

8. Wang MS, Xu G, Zhang ZJ, Guo GC (2010) Inorganic–organic hybrid photochromic materials. Chem Commun 46(3):361–376. doi:10.1039/b917890b

9. Liu SQ, Mohwald H, Volkmer D, Kurth DG (2006) Polyoxometalate-based electro- and photochromic dual-mode devices. Langmuir 22(5):1949–1951. doi:10.1021/la0523863

10. Liu SQ, Kurth DG, Bredenkotter B, Volkmer D (2002) The structure of self-assembled multilayers with polyoxometalate nanoclusters. J Am Chem Soc 124(41):12279–12287. doi:10.1021/ja026946l

11. Decher G (1997) Fuzzy nanoassemblies: toward layered polymeric multicomposites. Science 277(5330):1232–1237. doi:10.1126/science.277.5330.1232

12. Guo WH, Xu L, Li FY, Xu BB, Yang YB, Liu SP, Sun ZX (2010) Chitosan-assisted fabrication and electrocatalytic activity of the composite film electrode of heteropolytungstate/carbon nanotubes. Electrochim Acta 55(5):1523–1527. doi:10.1016/j.electacta.2009.10.003

13. Elsabee MZ, Naguib HF, Morsi RE (2012) Chitosan based nanofibers, review. Mater Sci Eng C 32(7):1711–1726. doi:10.1016/j.msec.2012.05.009

14. Ekrami-Kakhki M-S, Khorasani-Motlagh M, Noroozifar M (2011) Platinum nanoparticles self-assembled onto chitosan membrane as anode for direct methanol fuel cell. J Appl Electrochem 41(5):527–534

15. Prashanth KVH, Tharanathan RN (2007) Chitin/chitosan: modifications and their unlimited application potential—an overview. Trends Food Sci Technol 18(3):117–131. doi:10.1016/j.tifs.2006.10.022

16. Shahidi F, Arachchi JKV, Jeon YJ (1999) Food applications of chitin and chitosans. Trends Food Sci Technol 10(2):37–51. doi:10.1016/s0924-2244(99)00017-5

17. Alpat Ş, Alpat SK, Dursun Z, Telefoncu A (2009) Development of a new biosensor for mediatorless voltammetric determination of hydrogen peroxide and its application in milk samples. J Appl Electrochem 39(7):971–977

18. Liu SP, Xu L, Li FY, Guo WH, Xing Y, Sun ZX (2011) Carbon nanotubes-assisted polyoxometalate nanocomposite film with enhanced electrochromic performance. Electrochim Acta 56(24):8156–8162. doi:10.1016/j.electacta.2011.05.131

19. Fan DW, Hao JC (2009) Fabrication and electrocatalytic properties of chitosan and keplerate-type polyoxometalate $Mo_{72}Fe_{30}$ hybrid films. J Phys Chem B 113(21):7513–7516. doi:10.1021/jp901413w

20. Feng YH, Han ZG, Peng J, Lu J, Xue B, Li L, Ma HY, Wang EB (2006) Fabrication and characterization of multilayer films based on Keggin-type polyoxometalate and chitosan. Mater Lett 60(13–14):1588–1593. doi:10.1016/j.matlet.2005.11.069

21. Gaunt AJ, May I, Sarsfield MJ, Collison D, Helliwell M, Denniss IS (2003) A rare structural characterisation of the phosphomolybdate lacunary anion, $[PMo_{11}O_{39}]^{7-}$. Crystal structures of the Ln(III) complexes, $(NH_4)_{11}$ $[Ln(PMo_{11}O_{39})_2]·16H_2O$ (Ln = Ce-III, Sm-III, Dy-III or Lu-III). Dalton Trans 13:2767–2771. doi:10.1039/b301995k

22. Copping R, Gaunt AJ, May I, Sarsfield MJ, Collison D, Helliwell M, Denniss IS, Apperley DC (2005) Trivalent lanthanide lacunary phosphomolybdate complexes: a structural and spectroscopic study across the series $[Ln(PMo_{11}O_{39})_2]^{11-}$. Dalton Trans 7:1256–1262. doi:10.1039/b500408j

23. Fernandes DM, Cunha-Silva L, Ferreira RAS, Balula SS, Carlos LD, de Castro B, Freire C (2013) Redox behaviour, electrochromic properties and photoluminescence of potassium lanthano phosphomolybdate sandwich-type compounds. RSC Adv 3(37):16697–16707. doi:10.1039/c3ra41697f

24. Camilo CS, dos Santos DS, Rodrigues JJ, Vega ML, Campana SP, Oliveira ON, Mendonca CR (2003) Surface-relief gratings and photoinduced Birefringence in layer-by-layer films of chitosan and an azopolymer. Biomacromolecules 4(6):1583–1588. doi:10.1021/bm034220r

25. Koenig JF, Martel D (2008) Applying UV–Vis spectroscopy to step-by-step molecular self assembly on surface: does it bring pertinent information? Thin Solid Films 516(12):3865–3872. doi:10.1016/j.tsf.2007.07.137

26. Cheng L, Cox JA (2002) Nanocomposite multilayer film of a ruthenium metallodendrimer and a Dawson-type polyoxometalate as a bifunctional electrocatalyst. Chem Mater 14(1):6–8. doi:10.1021/cm010854y

27. Finsgar M, Fassbender S, Hirth S, Milosev I (2009) Electrochemical and XPS study of polyethyleneimines of different molecular sizes as corrosion inhibitors for AISI 430 stainless steel in near-neutral chloride media. Mater Chem Phys 116(1):198–206. doi:10.1016/j.matchemphys.2009.03.010

28. Perez-Romo P, Potvin C, Manoli JM, Chehimi MM, Djega-Mariadassou G (2002) Phosphorus-doped molybdenum oxynitrides and oxygen-modified molybdenum carbides: synthesis, characterization, and determination of turnover rates for propene hydrogenation. J Catal 208(1):187–196. doi:10.1006/jcat 2002.3564

29. Feng W, Ding YS, Liu Y, Lu R (2006) The photochromic process of polyoxometalate-based nanocomposite thin film by in situ AFM and spectroscopy. Mater Chem Phys 98(2–3):347–352. doi:10.1016/j.matchemphys.2005.09.037

30. Fernandes DM, Juliao D, Pereira C, Ananias D, Balula SS, Freire C (2012) Hybrid layer-by-layer films based on lanthanide-bridged silicotungstates and poly(ethylenimine). Colloids Surf A 415:302–309. doi:10.1016/j.colsurfa.2012.09.053

31. Le FH, Wang LX, Jia W, Jia DZ, Bao SJ (2012) Synthesis and photoluminescence of Eu^{2+} by co-doping Eu^{3+} and Cl^- in

Sr$_2$P$_2$O$_7$ under air atmosphere. J Alloys Compd 512(1):323–327. doi:10.1016/j.jallcom.2011.09.088

32. Durr H, Bouas-Laurent H (1990) Photochromism: molecules and systems. Elsevier, New York

33. Fernandes DM, Cunha-Silva L, Ferreira RAS, Balula SS, Carlos LD, Castro B, Freire C (2013) Redox behaviour, electrochromic properties and photoluminescence of potassium lanthano phosphomolybdate sandwich-type compounds. RSC Adv. doi:10.1039/C3RA41697F

34. Fernandes DM, Brett CMA, Cavaleiro AMV (2011) Layer-by-layer self-assembly and electrocatalytic properties of poly(ethylenimine)-silicotungstate multilayer composite films. J Solid State Electrochem 15(4):811–819. doi:10.1007/s10008-010-1154-1

35. Harris JJ, Bruening ML (2000) Electrochemical and in situ ellipsometric investigation of the permeability and stability of layered polyelectrolyte films. Langmuir 16(4):2006–2013. doi:10.1021/la990620h

36. Pardo-Yissar V, Katz E, Lioubashevski O, Willner I (2001) Layered polyelectrolyte films on Au electrodes: characterization of electron-transfer features at the charged polymer interface and application for selective redox reactions. Langmuir 17(4):1110–1118. doi:10.1021/la000729l

37. Farhat TR, Schlenoff JB (2001) Ion transport and equilibria in polyelectrolyte multilayers. Langmuir 17(4):1184–1192. doi:10.1021/la001298

38. Fernandes DM, Carapuca HM, Brett CMA, Cavaleiro AMV (2010) Electrochemical behaviour of self-assembly multilayer films based on iron-substituted alpha-Keggin polyoxotungstates.

Thin Solid Films 518(21):5881–5888. doi:10.1016/j.tsf.2010.05.065

39. Chu Y, Kim J, Choi S, Rhee CK (2011) Electron transfer behavior at polyoxometalate-adsorbed alkanethiol self-assembled monolayers. Appl Surf Sci 257(22):9490–9497. doi:10.1016/j.apsusc.2011.06.042

40. Gao SY, Li TH, Li X, Cao R (2006) Electrochemical behavior and multilayer films of the sandwich-type polyoxotungstate complex {K$_{10}$Co$_4$(H$_2$O)$_2$(PW$_9$O$_{34}$)$_2$}. Mater Lett 60(29–30):3622–3626. doi:10.1016/j.matlet.2006.03.104

41. Barreira SVP, Garcia-Morales V, Pereira CM, Manzanares JA, Silva F (2004) Electrochemical impedance spectroscopy of polyelectrolyte multilayer modified electrodes. J Phys Chem B 108(46):17973–17982. doi:10.1021/jp0466845

42. Yang GC, Gong H, Yang R, Guo HW, Wang YZ, Liu BF, Dong S (2006) Modification of electrode surface through electrospinning followed by self-assembly multilayer film of polyoxometalate and its photochromic. Electrochem Commun 8(5):790–796. doi:10.1016/j.elecom.2006.03.019

43. Qi W, Li HL, Wu LX (2008) Stable photochromism and controllable reduction properties of surfactant-encapsulated polyoxometalate/silica hybrid films. J Phys Chem B 112(28):8257–8263. doi:10.1021/jp801188e

44. Chen ZH, Loo BH, Ma Y, Cao YW, Ibrahim A, Yao JN (2004) Photochromism of novel molybdate/alkylamine composite thin films. ChemPhysChem 5(7):1020–1026. doi:10.1002/cphc.200400041